HHS Public Access

Author manuscript

*Nat Struct Mol Biol*. Author manuscript; available in PMC 2014 August 01.

Published in final edited form as:

*Nat Struct Mol Biol*. 2014 February ; 21(2): 133–142. doi:10.1038/nsmb.2762.

# *In vitro* membrane reconstitution of the T cell receptor proximal signaling network

**Enfu Hui**[1,2] and **Ronald D. Vale**[1,2]

[1]The Howard Hughes Medical Institute, University of California, San Francisco, San Francisco, California, USA

[2]Department of Cellular and Molecular Pharmacology, University of California, San Francisco, San Francisco, California, USA

## Abstract

T-cell receptor (TCR) phosphorylation is controlled by a complex network that includes Lck, a Src family kinase (SFK), the tyrosine phosphatase CD45, and the Lck-inhibitory kinase Csk. How these competing phosphorylation and dephosphorylation reactions are modulated to produce T-cell triggering is not fully understood. Here we reconstituted this signaling network using purified enzymes on liposomes, recapitulating the membrane environment in which they normally interact. We demonstrate that Lck's enzymatic activity can be regulated over a ~10-fold range by controlling its phosphorylation state. By varying kinase and phosphatase concentrations, we constructed phase diagrams that reveal ultrasensitivity in the transition from the quiescent to the phosphorylated state and demonstrate that coclustering TCR-Lck or detaching Csk from the membrane can trigger TCR phosphorylation. Our results provide insight into the mechanism of TCR signaling as well as other signaling pathways involving SFKs.

## INTRODUCTION

Regulation of protein phosphorylation underlies many signal transduction pathways that govern cellular processes. One well-studied signal transduction cascade is the T cell adaptive immune response, which is initiated by the interaction of the T cell receptor (TCR) with major histocompatibility complex-bound peptides (pMHC) on an antigen presenting cell (APC). The immediate consequence of TCR-pMHC binding is the tyrosine (Y) phosphorylation of the immunoreceptor tyrosine-based activation motifs (ITAMs) of the TCR complex. The phospho-ITAMs recruit the cytosolic protein tyrosine kinase ZAP-70, which subsequently catalyzes additional phosphorylation reactions to turn on downstream signaling cascades.



Correspondence: vale@ucsf.edu.

AUTHOR CONTRIBUTIONS

E.H. and R.D.V designed the study. E.H collected the data and conducted the analyses. E.H. and R.D.V. wrote the manuscript.

COMPETING FINANCIAL INTERESTS

The authors declare no competing financial interests.

Unlike many receptors that contain an intrinsic tyrosine kinase domain, the TCR itself lacks kinase activity but harbors 10 ITAMs (20 potential tyrosine phosphorylation sites) on the CD3 subunits (γε, δε and ζζ pairs). TCR phosphorylation is principally carried out by the Src family kinase (SFK) Lck and reversed by the transmembrane phosphatase CD45. Therefore, Lck and CD45 form a minimal network that controls the phosphorylation state of TCR. Similar to other members of SFKs, Lck is attached to the inner leaflet of the plasma membrane via N-terminal myristoylation and palmitoylation. SFKs are believed to be reciprocally regulated by phosphorylation and dephosphorylation of two conserved tyrosine residues[1]: phosphorylation of a tyrosine at the C terminal tail (Y505) by the inhibitory kinase Csk (C terminal Src kinase)[2,3] leads to inhibition, due to intramolecular interaction of its SH2 with the phosphotyrosine[4,5], while autophosphorylation of the activation loop tyrosine (Y394) is thought to enhance the kinase activity. CD45, a highly abundant transmembrane tyrosine phosphatase required for T cell development and activation[6], dephosphorylates both regulatory tyrosines of Lck[7-9] as well as reversing the action of Lck by dephosphorylating the ITAMs of the TCR[10].

While this general qualitative model of the proximal TCR phosphorylation network is well established, a quantitative understanding of the reaction network is lacking. Studies of Lck regulation have been sparse and reported different results[8,11] and CD45 phosphatase's specificity for phospho-Lck (pY505 and pY394) and phospho-TCR has not been examined. Furthermore, the net effect of competing kinase–phosphatase reactions on substrate phosphorylation has not been examined *in vitro* for any SFK, nor have phosphorylation reaction kinetics been measured on membrane surfaces (their physiological environment). To develop a quantitative understanding and predictive mathematical models for TCR signaling[12], reinvestigation of Lck, Csk and CD45 regulation, substrate specificity and activity levels using homogeneous, purified proteins and kinetic enzymatic readouts is warranted[13].

Here, we set out to reconstitute the TCR proximal signaling network consisting of Lck, Csk, CD45 and a TCR subunit (CD3ζ) onto the membranes of unilamellar liposomes and developed fluorescence readouts of phosphorylation. This reconstitution system has allowed us to control the 2-D concentration of each protein, and build the network in a stepwise fashion with increasing complexity. Using purified Lck with distinct phosphorylation states, we have been able to probe the regulatory mechanism of Lck in its native membrane environment. We also have characterized individual enzymatic reactions in isolation as well as in combination to construct phase diagrams of the TCR-kinase-phosphatase network to understand how the system is maintained at a quiescent state and how it might be activated by TCR ligation.

## RESULTS

### Membrane reconstitution of Lck phosphorylation of CD3ζ

In order to study Lck catalyzed phosphorylation of ITAMs in a membrane environment, we first reconstituted Lck and its substrate CD3ζ onto artificial lipid bilayers. Lck is anchored to the inner leaflet of the plasma membrane through myristoylation of a conserved N terminal glycine[14]. We replaced the N-terminal glycine with decahistidine ($His_{10}$) tag so that Lck

could be bound to liposomes containing DGS-NTA-Ni lipids (see **Online Methods**). An N-terminal $His_{10}$ tag was similarly placed on the cytosolic domain of recombinant CD3ζ. Using a Föster resonance energy transfer (FRET) based assay, we found that $His_{10}$-tagged proteins stably bind to these liposomes with a $K_d$ of 0.6 nM and an off-rate of 0.0009 $s^{-1}$ (**Supplementary Fig. 1a,b**), in agreement with a previous study[15].

To monitor the phosphorylation state of CD3ζ, we generated a fluorescently-labeled, SNAPtag fusion protein of tSH2 of ZAP70 (designated as $SNAP_{505}$-tSH2) that binds doubly phosphorylated ITAMs on CD3ζ (**Fig. 1a**). Upon addition of ATP, phosphorylation of CD3ζ by Lck leads to recruitment of $SNAP_{505}$-tSH2 to liposomes, as detected by FRET between $SNAP_{505}$-tSH2 (donor) and rhodamine-conjugated lipids (acceptor) (**Fig. 1b**; decrease in donor fluorescence). Immunoblotting revealed a similar time-dependent phosphorylation of CD3ζ (**Fig. 1c**), indicating that the FRET assay faithfully reports the phosphorylation of CD3ζ and that the presence of $SNAP_{505}$-tSH2 does not interfere with the rate of the overall reaction.

## Membrane attachment accelerates Lck phosphorylation of CD3ζ

Mathematical modeling predicts that bimolecular reaction rates are much greater on membrane surfaces than in solution, since the diffusional search is confined to two dimensions[16,17]. Indeed, Ras activation by Son of sevenless (SOS) was found to occur 500-fold faster on artificial liposomes than in solution[18]. To compare the kinetics of Lck catalyzed CD3ζ phosphorylation on membranes versus in solution, we measured FRET between tetramethylrhodamine bound to CD3ζ and $SNAP_{505}$-tSH2 (see **Online Methods**). Similarly, we found that pre-binding both Lck and CD3ζ to liposomes at their physiological densities (300 and 250 $\mu m^{-2}$ respectively, **Online Methods**) led to several hundred-fold faster phosphorylation rates than in solution and that the phosphorylation rate exhibited a positive correlation with the protein densities (**Fig. 1d**).

Recently, it was reported that acidic phospholipids bind to CD3 chains in resting T cells, thereby limiting the access of Lck to ITAMs[19,20]. In contrast, we found here that CD3ζ phosphorylation occurred 1.8-fold faster on membranes with 10% phosphatidylserine (PS) (an acidic phospholipid) versus no PS; 20% PS did not further increase the rate (**Supplementary Fig. 1c**). We note that previous studies[19,20] utilized the soluble cytosolic portion of CD3, whereas we pre-anchored CD3ζ chains to the membrane, mimicking the situation in cells. For the liposome assays in this study, we used 10% PS (see **Online Methods**), which is close to the concentration in the plasma membrane inner leaflet of human T cells (7.4% PS)[21].

## Lck autophosphorylates both Y394 and Y505 in trans

Phosphorylations of two conserved tyrosines in SFKs play distinct roles in kinase regulation. Phosphorylation of a tyrosine (Y505 in Lck) near the C terminus leads to its intramolecular binding to the SH2 domain, resulting in a closed, inactive conformation of the kinase[4,5]. In contrast, phosphorylation of a tyrosine (Y394 in Lck) in the activation loop leads to kinase activation[22]. It is generally believed that Y394 is autophosphorylated *in trans*[14], whereas Y505 phosphorylation is catalyzed by Csk, a negative regulatory kinase[23]. Whether this is

the sole mechanism for Y505 phosphorylation is unclear, with some prior studies suggesting that c-Src is capable of autophosphorylating Y527[24,25].

In order to clarify its mechanism of autophosphorylation, we incubated Lck with ATP and measured the phosphorylation of Y394 and Y505 over time with phosphospecific antibodies. The rate of Y394 phosphorylation was at least 100-fold faster on membranes ($t_{1/2}$ < 0.25 and >10 min on membranes and in solution; respectively, **Fig. 2a**). The massive rate enhancement upon membrane attachment suggests that Lck phosphorylates Y394 *in trans*.

We also observed a time-dependent increase in Y505 phosphorylation (**Fig. 2a**), indicating autophosphorylation on this tyrosine. The $K_{M\text{-}ATP}$ for Y505 phosphorylation (10 μM) was 45-fold higher than Y394 phosphorylation (0.22 μM). Interestingly, Y394F mutation further increased the $K_{M\text{-}ATP}$ for Y505 phosphorylation by 5-fold (50 μM) (**Fig. 2c**), indicating that phosphorylation of Y394 increases the ATP sensitivity for subsequent Y505 phosphorylation (see **Supplementary Fig. 2a-c** for the time course of autophosphorylation at four ATP concentrations). The much higher $K_{M\text{-}ATP}$ for Y505 phosphorylation may explain why it was undetected in previous *in vitro* studies; however, the *in vivo* ATP concentration (1-10 mM) is more than sufficient for this phosphorylation to occur.

Y505 phosphorylation was only modestly increased by anchoring Lck onto liposomes (**Fig. 2a**), an observation that might suggest an intramolecular phosphorylation. To test whether Lck autophosphorylates Y505 *in cis*, we mixed equal concentrations of wild-type (WT) Lck and a kinase-dead (K273R) Lck mutant on liposomes and examined their autophosphorylation kinetics (**Fig. 2b**). In this mixture, the phosphorylation of Y394 and Y505 on K273R can only occur *in trans*. We observed that phosphorylation of both Y505 and Y394 occurred at indistinguishable rates for the two versions of Lck (**Fig. 2b**, right). From this experiment, we conclude that Lck autophosphorylates both Y394 and Y505 *in trans*.

## Quantitation of the magnitude of phospho-regulation of Lck

In order to determine the effects of phosphorylation on Lck kinase activity, a comparison of monomeric Lck with distinct, well-defined phosphorylation states is required. To this end, we have measured the enzyme kinetics of membrane-attached Lck in the unphosphorylated (designated as Apo, prepared by CD45 treatment; **Supplementary Fig. 2d** and **Online Methods**), monophophosporylated (pY394 or pY505), and doubly phosphorylated (pY394-pY505) states. We prepared doubly phosphorylated Lck by incubating purified Lck with ATP until both Y505 and Y394 reached a maximum level (**Online Methods, Supplementary Fig. 2e,f**). Mass spectrometry revealed 82% and 97% phosphorylation on Y394 and Y505, respectively (**Supplementary Fig. 3**), suggesting that at least 79%-82% Lck was doubly phosphorylated. Monophosphorylated Lck was similarly produced by autophosphorylation, with phosphorylation at one site blocked by either Y394F or Y505F mutation. We measured the phosphorylation kinetics of CD3ζ by FRET over a wide range of substrate concentrations, and plotted the initial rates ($v_0$) of phosphorylation as a function of CD3ζ concentration (**Supplementary Fig. 4a,b**). Data were fit with a Hill-equation-

modified Michelis-Menten model (**Fig. 3a,b**), yielding $k_{cat}$, $K_M$ and the Hill coefficients ($n_H$) (**Table 1**). The observed $k_{cat}$ values varied from 1-7 $s^{-1}$, in the same range as solution measurements on recombinant WT Lck using a peptide substrate corresponding to the autophosphorylation site of c-Src[26], but orders of magnitude higher than a recent study using peptide substrates corresponding to individual tyrosines in CD3ζ[27]. The apparent 2-D $K_M$ values (200-500 $\mu m^{-2}$) are similar to physiological densities of CD3ζ (100-360 $\mu m^{-2}$), suggesting that Lck is operating in T cells at almost its maximal capacity while maintaining sensitivity to changes in the substrate concentration.

Our analysis of the catalytic activity ($k_{cat}/K_M$) shows that tyrosine mutations themselves do not alter kinase activity, since the Y394F-Y505F double mutant and WT, dephosphorylated Lck (designated as Apo) exhibited similar catalytic activities for CD3ζ (see **Supplementary Note** for comparison with prior findings of these mutants). However, pre-phosphorylation of Y394 (in the Y505F background) enhanced the catalytic activity by 70%; in contrast, phosphorylation of Y505 (in the Y394F background) decreased the catalytic activity by 83%. Interestingly, when both tyrosines were phosphorylated, the catalytic activity returned to the unphosphorylated kinase level, suggesting that the inhibitory effect of Y505 can be overcome by Y394 phosphorylation, in agreement with a recent study using immunoprecipitated Lck[28].

## Lck phosphorylates CD3ζ in a largely non-processive manner

c-Src was reported to catalyze the multisite phosphorylation of a synthetic peptide[29] or p130Cas[30] through a processive mechanism. Since CD3ζ contains six phosphorylatable tyrosines, we wished to determine whether Lck carries out multisite phosphorylation in a processive or non-processive (distributive) manner. Phosphorylation of CD3ζ resulted in slower eletrophoretic mobility[31], enabling identification of intermediates between the non-phosphorylated and fully phosphorylated (6 pY) state. After addition of ATP to membrane-attached CD3ζ and Lck, we observed a time-dependent, upward shift of the CD3ζ band with clear intermediates (**Fig. 3c**). This result argues against a processive mechanism, which often leads to an abrupt transition between the unphosphorylated and fully phosphorylated species[32].

We also examined the rate of formation of the fully phosphorylated product at different substrate concentrations. A processive kinase remains bound to the substrate, phosphorylating all the sites in one encounter; as a result, the onset of the fully phosphorylated substrate is independent of the substrate concentration. Conversely, in a distributive mechanism in which the formation of the fully phosphorylated product requires repetitive binding interactions between kinase and the same substrate, the encounter of a kinase with a partially phosphorylated substrate is decreased at higher substrate concentration due to peer competition. We found that increasing the CD3ζ concentration by 3-fold considerably delayed the formation of the fully phosphorylated product than at lower substrate concentration (**Fig. 3c**), consistent with a non-processive (or distributive) mechanism. The processivity of Src has been attributed to its SH2 domain, which can potentially bind, *in trans*, to the phosphotyrosines in the partially phosphorylated substrate[29]. However, we find that a SH2 deletion (△SH2) mutant of Lck produces a similar

diffusive pattern of the phosphorylation products, except with slightly faster kinetics than the WT kinase (**Fig. 3d**). Collectively, these data suggest that Lck phosphorylates CD3ζ in a largely non-processive manner, although we cannot rule out processive phosphorylation for the intact, multi-subunit TCR.

## CD45 enzymatic activity

Although both Lck and CD3ζ are known substrates for CD45, the relative substrate specificity has not been determined in a quantitative manner. Using a recombinant cytoplasmic portion of CD45, we probed the time course of dephosphorylation of Lck-Y394, Lck-Y505 and CD3ζ on liposome membranes. CD3ζ was dephosphorylated >20-fold faster than Lck by CD45 (**Fig. 4a,b**), indicating that it is a much better substrate. Lck-Y394 and Lck-Y505 were dephosphorylated at similar rates. Notably, the presence of tSH2 of ZAP70 dramatically reduced the kinetics of CD45 mediated CD3ζ dephosphorylation (**Fig. 4a,c**), indicating that phospho-ITAMs can be protected from CD45 by bound ZAP-70.

## Phase diagrams of the Lck-CD45-CD3ζ network

Understanding how the combined actions of kinases and phosphatases affect the output of signaling pathways is nontrivial, due to the presence of the many regulatory reactions and the lack of knowledge of reaction rate constants (**Fig. 5a**). Here, we determined the combinatorial effects of Lck (WT or phosphorylation mutants) and CD45 on the phosphorylation of TCR on a membrane, by mapping the phase diagram of the network (**Fig. 5a**). In this experiment, the substrate CD3ζ was kept at a fixed density (~400 molecules per $\mu m^2$, **Online Methods**), whereas the concentrations of both Lck and CD45 were varied over two to three orders of magnitude (84 conditions). The level of CD3ζ phosphorylation at 1 h was probed by FRET as described in **Fig. 1a**, plotted against Lck and CD45 surface densities, and converted into a heat map (**Fig. 5b,c**, left, red-blue: high to low phosphorylation). We note that a steady state was not reached in all conditions at 1 h (**Fig. 5b**), and end point data at 0.5, 1.5, and 2 h produced slightly shifted heat maps (**Supplementary Fig. 5a-d**) but did not change the general conclusions. At equal Lck and CD45 densities (black dashed line), CD3ζ phosphorylation remained strong. Increasing the Lck density enhanced the extent of CD3ζ phosphorylation, whereas increasing the CD45 density did the opposite, suggesting the predominant effect of CD45 on CD3ζ phosphorylation is inhibitory. At the physiological relevant regime (indicated by a red dashed box), little to no phosphorylation of CD3ζ was observed. Mutating the activating tyrosine (Y394F) shrank the phosphorylation positive region considerably (**Fig. 5c**, middle). Conversely, the constitutively active Lck mutant (Y505F) expanded the phosphorylation positive region, indicative of a higher kinase activity (**Fig. 5c**, right). These differences reflect the contribution of Lck autophosphorylation on the phase behavior of the network.

To determine whether there is an ultrasensitive concentration dependence, we plotted CD3ζ phosphorylation as a function of WT Lck to CD45 molar ratios (Lck/CD45, **Fig. 5d**), as described for other competing kinase-phosphatase reactions[33]. The $n_H$ of this plot (~2.2) suggests a switch-like behavior. The half maximal CD3ζ phosphorylation for Lck (WT) occurs at a ratio of 0.68. We also examined the CD3ζ phosphorylation as a function of varying Lck or CD45 concentration, keeping the opposing enzyme at a fixed concentration

(**Fig. 5e,f**). The $n_H$ for Lck activation was ~1.7 at two different CD45 densities of 30 $\mu m^{-2}$ and 600 $\mu m^{-2}$, the latter being the physiological level in T cells (see **Online Methods**). Mutating either Y394 or Y505 to phenylalanine did not substantially alter the $n_H$ of dose response plots (**Supplementary Fig. 5e-j**), suggesting that the phospho-regulation of Lck is not the major source of this cooperativity. In contrast, when CD45 was varied at two fixed Lck concentrations (20 $\mu m^{-2}$ and 200 $\mu m^{-2}$, the latter being physiological), a more switch-like response was observed ($n_H$ = 2.8 and 2.9 respectively) (**Fig. 5f**). We were concerned that this switch-like behavior might be affected by the presence of the $SNAP_{505}$-tSH2 reporter which can protect CD3ζ from CD45 dephosphorylation (**Fig. 4b,c**), but found that the reporter did not affect the $n_H$ of this reaction (**Fig. 5g**). Taken together, these data suggest that decreasing CD45 level or activity, rather than increasing Lck, provides a more effective way to trigger TCR phosphorylation.

## Regulation by the inhibitory kinase Csk

Csk plays an important negative regulatory role in signaling by phosphorylating Lck on Y505[23]. Membrane-bound Csk (~500 $\mu m^{-2}$) accelerated Y505 phosphorylation by ~12-fold, but had little effect on the rate of Y394 phosphorylation (**Fig. 6a**). Reducing the Lck density to ~50 $\mu m^{-2}$ in the presence of Csk (~500 $\mu m^{-2}$) only slightly accelerated the phosphorylation of Y505, but substantially retarded Y394 phosphorylation (**Fig. 6b**). We also repeated the experiments in solution, and confirmed the finding that Csk not only promotes the phosphorylation of Y505, but also inhibits the phosphorylation of Y394 (**Supplementary Fig. 6**). Since Lck phosphorylates Y394 *in trans*, we propose that a lower ratio of Lck to Csk kinetically favors initial Y505 phosphorylation, which would inactivate a subpopulation of Lck and in turn decrease the kinetics of *trans*-autophosphorylation on Y394 by reducing the active kinase on the membrane.

We next determined how Csk affects the net outcome of Lck phosphorylation of CD3ζ. Somewhat surprisingly, Csk (~500 $\mu m^{-2}$) was capable of phosphorylating CD3ζ in the absence of Lck, although with a long latency (~5 min) and slow kinetics (**Supplementary Fig. 7a**, $t_{1/2} \approx 28$ min). Combining Lck and Csk (both at ~500 $\mu m^{-2}$) reduced the rate of CD3ζ phosphorylation by ~36% as compared to WT Lck alone (**Supplementary Fig. 7b**, $t_{1/2}$ values: 1.1 min for “Lck + Csk” and 0.7 min for “Lck”), demonstrating the inhibitory effect of Csk on Lck. At an order of magnitude lower Lck density (50 $\mu m^{-2}$, **Supplementary Fig. 7c**), we found a much stronger inhibitory effect of Csk on Lck (69% slower CD3ζ phosphorylation). This result is consistent with the idea that rapid Y394 phosphorylation at high Lck densities (**Fig. 2**) partially overrides the inhibitory effect of Csk. Consistent with a protective role of Lck pY394, the Y394F mutation led to much greater inhibitory effect of Csk, reducing the rate of CD3ζ phosphorylation by 84% (**Supplementary Fig. 10b**); as expected Y505F completely abolished the effect of Csk at all Lck densities (**Supplementary Fig. 7b,c**). We conclude that Csk inhibits the catalytic activity of Lck mainly through increasing Y505 phosphorylation.

We next determined how Csk alters the phase behavior for phosphorylation state of CD3ζ by using fixed concentrations of Csk (~150 $\mu m^{-2}$) and CD3ζ (~400 $\mu m^{-2}$) and varying the concentrations of Lck and CD45. The presence of Csk shrank the “phosphorylation positive”

area compared to the system lacking Csk (**Fig. 6c**), thus demonstrating the negative role of Csk. We note that while Csk reduced the phosphorylation signal under most conditions, it enhanced the CD3ζ phosphorylation at low densities of both Lck and CD45 (lower left corner of the diagram). This apparent positive role of Csk is because Csk alone can directly phosphorylate CD3ζ (**Supplementary Fig. 7a**).

## Membrane detachment of Csk triggers CD3ζ phosphorylation

TCR stimulation by antibody causes transient dissociation Csk from its transmembrane adaptor protein PAG (CBP)[34,35]. This cytosolic translocation event has been proposed to trigger or augment TCR signaling by releasing Lck inhibition (phosphorylation of Y505)[23], which is consistent with recent data showing that acute inhibition of membrane-targeted Csk leads to T cell activation[36]. To test this idea in our reconstitution system, we induce Csk dissociation in a controlled manner by using TVMV protease to cleave Csk from its $His_{10}$-tag that anchors it to the membrane (**Fig. 6d**). When Csk, Lck, CD45 and CD3ζ were reconstituted to liposomes in a regime of the phase diagram that produces little phosphorylation (**Fig. 6c**, right), subsequent addition of the TVMV protease caused a robust and rapid phosphorylation of CD3ζ (**Fig. 6d**, black). These *in vitro* data provide direct evidence that Csk dissociation from the membrane is sufficient for triggering TCR phosphorylation in a physiological regime of CD45 and Lck concentrations on the membrane.

## Protein clustering triggers CD3ζ phosphorylation

Upon TCR engagement, signaling proteins, such as Lck and ZAP-70, rapidly segregate into discrete microdomains that exclude the phosphatase CD45[37-39], resulting in local concentration changes of these proteins. Our phase diagrams (**Fig. 5c)** predict that a small perturbation in the kinase or phosphatase concentration could drive a phase transition of the network, leading to net TCR phosphorylation. To test this idea, we established an inducible protein clustering system on the liposome surface by fusing Lck and CD3ζ to repeats of FKBP ($FKBP_6$) and FRB ($FRB_4$). Addition of rapamycin would trigger the formation of high affinity FKBP-rapamycin-FRB complexes[40], thereby creating multivalent heteromers of these fusion proteins (**Fig. 7a**). In the absence of rapamycin, no phosphorylation was observed at physiological densities of Lck and CD45 (**Fig. 7b**). Strikingly, rapamycin addition greatly expanded the “phosphorylation positive” area, allowing strong phosphorylation to occur at even the highest CD45 density tested (3,000 $\mu m^{-2}$). While we could not directly observe clustering in the liposomes after rapamycin due to their size (~200 nm), this strong effect on the phase diagram is most likely due to multimerization of FKBP-FRB chimeric proteins, as documented for other multivalent protein interactions[41].

TCR clusters have also been detected in quiescent T cells using superresolution microscopy[42,43], but the effects of such clustering are unknown. We next determined how clustering of CD3ζ alone (using $FKBP_6$-CD3ζ and $FRB_4$-CD3ζ) affects the phase behavior of the kinase-phosphatase system (**Fig. 7c**). Addition of rapamycin to precluster the substrate CD3ζ increased the “phosphorylation positive” area, particularly at relatively high Lck concentrations. However, physiologically relevant concentrations of CD45 (360-1,800 $\mu m^{-2}$) were sufficient to keep the system quiescent, even in presence of rapamycin.

## DISCUSSION

In this work, we analyzed the TCR proximal signaling network reconstituted onto lipid bilayers, first decoupling this complex network into sub-reactions involving either the kinase or phosphatase and then combining components to reconstruct a more complete system. Prior studies on the mechanism of Lck, Csk, and CD45 were mainly on cellular systems, using knockdowns or mutations, or single time point phosphosphorylation readouts from immunoprecipitation reactions. While such work can provide a cellular context for the roles of the enzymes, it is difficult to control enzyme states (e.g. regulatory phosphorylation states of Lck) and levels, and hence to obtain precise kinetic information of rates and equilibrium measurements. Our work provides a complementary approach to those cellular studies by using purified enzymes in well-defined *in vitro* reactions. While lacking cellular complexity, we feel that our system provides information that is relevant for understanding how these enzymes function in living cells. First, unlike all prior *in vitro* studies of SFKs, our reconstitution system studies how these enzymes work on membrane surfaces, where reaction rates and potentially substrate presentation differ from solution measurements. Second, we used an intact, native polypeptide (CD3ζ of the TCR) as a substrate for the reaction. While this is a simplification of the multi-subunit TCR complex, CD3ζ is sufficient to initiate signaling in chimeric antigen receptors[44] and represents a more physiological substrate than denatured enolase or peptides, which have been widely used for studying SFKs. Third, when physiological concentrations of Lck, CD45 and CD3ζ in mature T cells are used in our liposome-based reaction, the network is in a quiescent state but is poised close to a threshold point for net CD3ζ phosphorylation, thus mimicking the physiological situation for this enzyme network. Importantly, by varying the concentrations of purified enzymes, combining them in different ways, and performing kinetic and steady state readouts, we have gained new insights into the substrate specificity, enzyme regulation, and how the proximal TCR signaling system behaves as a network.

### Kinase and phosphatase specificity and regulation

A general consensus is that the kinase activity of all SFKs is differentially regulated by phosphorylation of two conserved tyrosines[1]. This notion is largely based on end-point kinase assays of WT and tyrosine mutants of Src immunoprecipitated from cell lysates[45-49]. While Y527F mutation was consistently found to increase the activity of immunoprecipitated c-Src, the Y416F did not produce any effect on c-Src activity[47-49] but caused an 80% reduction in v-Src activity[50]. Two similar studies on Lck regulation also lead to conflicting results regarding how tyrosine mutations affect Lck activity[8,11] (see **Supplementary Note** for a detailed review of *in vitro* studies on SFKs regulation). These discrepancies were likely due to the mixed phosphorylation states of the kinase-antibody immunocomplex, the use of different substrates and the lack of kinetic information of the end point measurements.

In the present study using purified Lck with distinct phosphorylation states, we have placed quantitative values on these two regulatory effects on Lck: a 70% increase and an 83% decrease in the kinase activity upon Y394 and Y505 phosphorylation respectively, revealing a 10-fold dynamic range in Lck activity (**Fig. 8**). Our measurements **(Fig. 3a,b)** suggest an

imbalance of the two opposing regulatory effects, as phosphorylation of Y394 causes only a modest activation while phosphorylation of Y505 produces a much stronger repression. Perhaps more important for signaling, our results indicate that the final Lck activity depends on the temporal order for the two phosphorylation events. If Y505 phosphorylation occurs first, the kinase becomes essentially inactive, which greatly reduces the likelihood for subsequent Y394 phosphorylation. However, if Y394 phosphorylation occurs first, Lck remains active when subsequently phosphorylated on Y505, in agreement with a previous study on other SFKs[51]. Thus, Y394 phosphorylation may serve a more important role in protecting the kinase from inactivation rather than in increasing kinase activity *per se* (< 2-fold effect). This would explain a previous finding that Y394 phosphorylation is absolutely required for initiation of T cell signaling[52]. Our results also reveal that conditions which favor Y505 versus Y394 phosphorylation will lead to Lck quiescence, particularly the combination of Csk and lower Lck concentrations. (**Fig. 6b** and **Supplementary Fig. 6b**).

We also observed features of Lck regulation that were not previously anticipated. It was thought that Lck autophosphorylates Y394 *in trans*, while Y505 phosphorylation solely relies on the inhibitory kinase Csk[23]. However, we find that Lck also autophosphorylates Y505 *in trans* (**Fig. 2**). While this result is surprising for current thinking of Lck regulation, it is consistent with previous findings that c-Src autophosphorylates Y527[24,46]. While our and prior studies showing autophosphorylation of the inhibitory tyrosine of SFKs were performed with purified proteins, evidence suggests that this reaction may also occur in cells. In support of this idea, we have found that treatment of Jurkat T cells with a Lck specific inhibitor (320-fold selectivity over Csk[53]) leads to up to 50% reduction in Y505 phosphorylation (**Supplementary Fig. 8**). Conversely, selective inhibition of Csk in T cells does not completely eliminate Lck Y505 phosphorylation[54] and 20-50% of c-Src Y527 phosphorylation persists in Csk deficient cells[3]. Interestingly, unlike *trans*-phosphorylation of Y394, the *trans*-autophosphorylation of Y505 (**Fig. 2b**) is only modestly enhanced by confining Lck to a two-dimensional membrane surface (**Fig. 2a**), perhaps due to a sub-optimal geometry for catalysis.

Our study also has uncovered new information on the substrate specificity of CD45. We show that CD45 dephosphorylates CD3ζ >20-fold faster than Lck, suggesting that CD45's dominant effect is reversing Lck's phosphorylation of the TCR. However, full inhibition of CD3ζ phosphorylation requires at least 10-fold higher CD45 than Lck (**Fig. 5d**), which may explain the very high expression of CD45 in mature T cells[55]. This high demand for CD45 may, in part, be due to ZAP70 binding protecting phospho-ITAMs against CD45 dephosphorylation (**Fig. 4a,c** and **Fig. 5g**). Regarding Lck, we show that CD45 dephosphorylates pY394 and pY505 at similar rates (**Fig. 4b,c**). The integrated action of all three CD45-catalyzed dephosphorylation events can be “visualized” from the phase diagrams, which reveal that CD45 is primarily an inhibitor for TCR phosphorylation (**Fig. 5c**).

## TCR triggering

Some element(s) in the T cell signaling pathway is believed to be highly cooperative, such that the transition from a quiescent to an activated T cell occurs in a switch-like manner. Our

data reported here have revealed that cooperativity is at least partially encoded in the TCR proximal signaling architecture itself. A recent mathematical model by Mukhopadyay et al.[12] suggested that the TCR proximal signaling ultrasensitivity arises from the multiple phosphoacceptor sites on CD3ζ, sequential phosphorylation of these sites by Lck[27], and protection from dephosphorylation by ZAP-70. We have obtained experimental support for ZAP-70 protection against CD45 dephosphorylation (**Fig 4a,c**) but found that the ability of ZAP-70 to bind phospho-ITAMs did not alter the cooperativity of the kinase-phosphatase reaction (**Fig. 5g**). We speculate that at least part of the switch-like behavior observed in this study may be due to the distributive multisite phosphorylation of CD3ζ by Lck, which has been suggested to produce ultrasensitivities in other kinase cascades[56], especially when both the substrate and enzyme are membrane-confined[57]. In this framework, increasing the number of phosphorylations (e.g. using an intact TCR complex that contains 10 ITAMs) might enhance the degree of ultrasensitivity.

Additional mechanisms for achieving greater ultrasensitivity could include spatial exclusion of CD45 from the tight contact zone of T lymphocytes and APCs[38,39], as was proposed in the "kinetic segregation model"[58,59]. Consistent with this idea, phosphorylation of CD3ζ exhibited a greater sensitivity to variation in CD45 concentration (**Fig. 5f**) than Lck concentration (**Fig. 5e**). We also show that inducing the clustering of Lck and CD3ζ using a chemically-inducible FKBP-FRB aggregation system triggered a dramatic, global phase transition of strong TCR phosphorylation at physiological levels of Lck and CD45 (**Fig. 7b**). In the future, other elements in the T cell signaling pathway, such as the adapter protein LAT and its associated factors, could be added to reconstituted liposomes to see how they affect the threshold and sensitivity of the TCR or downstream phosphorylation reactions.

## ONLINE METHODS

### Materials

Synthetic 1,2-dioleoyl-sn-glycero-3-phosphocholine (POPC), 1-palmitoyl-2-oleoyl-*sn*-glycero-3- phospho-L-serine (POPS), 1,2-dioleoyl-*sn*-glycero-3-[(N-(5-amino-1-carboxypentyl)iminodiacetic acid)succinyl] (nickel salt, DGS-NTA-Ni) and N-(lissamine rhodamine B sulfonyl)-1,2-dipalmitoylsn-glycero-3 phosphoethanolamine (Rhod-PE) were purchased from Avanti Polar Lipids. SNAP-cell 505 was obtained from New England Biolabs. Tetramethylrhodamine-5-maleimide was from Life Technologies. Lck inhibitor (7-Cyclopentyl-5-(4-phenoxyphenyl)-7H-pyrrolo[2,3-d]pyrimidin-4-ylamine) and rapamycin were obtained from Sigma-Aldrich. The antibodies used in this study were: mouse anti-pY142-CD3ζ (anti-CD247, 558489, 1:1000, BD PhosFlow), anti-pY418-Src (pY394-Lck, 560094, BD PhosFlow 1:500), anti-pY505-Lck (558552, BD PhosFlow, 1:3,000), anti-GAPDH (MAB374, Millipore, 1:50,000), rabbit anti-Lck (2984S, Cell signaling, 1:1,000), rabbit anti-pY416-Src (2101S, Cell signaling, 1:1,000). Validation of each antibody is provided on the manufacturer's websites.

### Recombinant protein expression and purification

cDNA encoding the cytosolic domain of human CD3ζ (aa52-164) was subcloned into pET28a vector. The coding sequence of the $His_6$ tag in pET28a was modified to $His_{10}$ via

Quikchange mutagenesis. A Lys-Cys-Lys-Lys sequence was inserted between $His_{10}$ and CD3ζ for fluorescent labeling of the protein product. Full length (FL) human Lck, FL human Csk, and the cytosolic portion of human CD45 (aa598-1304) were subcloned into a modified pFastBacHTA vector containing $His_{10}$ upstream to the multiple cloning site. For Lck, a G2A point mutation was introduced to prevent the N-terminal myristoylation and tyrosine mutants were generated by Quikchange. In order to create Lck or CD3ζ fusion proteins containing FKBP or FRB repeats. FKBP-L or FRB-L was flanked by XbaI and SpeI site, and repetitively cloned into the vector backbone at the SpeI site. “L” denotes a 12-aa flexible linker (GSGSGSGGGGSS). The SNAP-tSH2 reporter construct was generated by fusing the SNAP-tag (New England Biolabs), a 14-aa flexible linker (GSGSGSGGGGSSTR), and the tandem SH2 domains of human ZAP70 (aa1-259), and cloned into pGEX6P-2 vector via BamHI and EcoRI. Sequences of the primers for cloning are available upon request.

$His_{10}$-KKCK-CD3ζ were bacterially expressed in BL21(DE3) strain of *Escherichia coli*. $His_{10}$-tagged Lck, CD45, Csk, and all their fusion proteins were all expressed in SF9 cells using the Bac-to-Bac baculovirus system (Life Technologies). The cells were lysed in an Avestin Emulsiflex system. All $His_{10}$ proteins were purified by using Ni-NTA agarose essentially as described[60]. SNAP-tSH2 was expressed in BL21(DE3) as a glutathione S-transferase (GST) fusion protein and purified by using glutathione-Sepharose beads (GE healthcare) as described[61]. Soluble SNAP-tSH2 was generated by cleaving the GST moiety via the PreScission Protease.

For dephosphorylation of recombinant Lck as shown in **Supplementary Fig. 2d**, the cytosolic portion of CD45 (aa598-1304) was fused with a GST tag and preScission recognition site at its N terminus, and cloned into a modified pFastBacHTA vector lacking the coding sequence of the polyhistidine tag. The GST fusion protein (GST-CD45) was expressed in SF9 cells and purified using glutathione-Sepharose beads (GE healthcare) followed by elution with 10 mM glutathione and dialysis.

All affinity-purified proteins used in this study were subjected to gel filtration chromatography using a Superdex 200 10/300 GL column (GE healthcare) in HEPES-buffered saline (HBS) containing 50 mM HEPES-NaOH, pH 7.5, 150 mM NaCl, and 10% glycerol. The monomer fractions were pooled, snap frozen in liquid N2 and stored at —80 °C. All gel-filtered proteins were quantified by SDS-PAGE and Coomassie staining using BSA as a standard.

## Protein labeling

To prepare the fluorescent reporter for FRET assays, 10 μM SNAP-tSH2 were incubated with equal concentration of SNAP-cell 505 in HBS buffer for 1 h at room temperature or overnight on ice in the presence of 1 mM TCEP. For solution-based FRET as shown in **Fig. 1d,e**, 10 μM $His_{10}$-KKCKCD3ζ was incubated with 30 μM tetramethylrhodamine-5-maleimide in HBS buffer for 1 h at room temperature. The reaction was quenched by 1 mM DTT and the excess dyes were removed by extensive dialysis. The labeling efficiency was 80-90%.

### Liposome preparation

Phospholipids (79.7% POPC + 10% POPS + 10% DGS-NTA-Ni + 0.3% Rhod-PE) were dried under a stream of $N_2$, desiccated for 3 h and suspended in 1x Kinase buffer. Large unilamellar liposomes were prepared by extrusion through a pair of polycarbonate filters with a pore size of 200 nm, according to the manufacturer instructions (Avanti Polar Lipids). For liposomes used in **Supplementary Fig. 1c**, the changes in PS content were compensated by opposite changes in PC content.

### Prephosphorylation and dephosphorylation of Lck and CD3ζ

Recombinant Lck from SF9 cells was partially phosphorylated at Y505 (**Fig. 2a**, time zero). In order to prepare a homogeneous population of unphosphorylated Lck, freshly purified Lck was incubated with GST-CD45 on ice for at least 12 h for complete dephosphorylation (**Supplementary Fig. 2d**). Mass spectrometry revealed 0% phosphorylation on Y394 and 1.5% phosphorylation of Y505 after this treatment (E. Hui. and R.D. Vale, unpublished observation). The CD45 phosphatase was pulled down by glutathione-Sepharose beads, and the supernatant containing Lck and residual GST-CD45 was subjected to gel filtration for further separation.

In order to prephosphorylate Lck on either or both regulatory tyrosines (Y394 and Y505), freshly purified Lck (WT), Lck (Y394F) or Lck (505F) was concentrated using Amicon Ultra Centrifugal Filter units (Millipore) to > 5 μM, and mixed with 1 mM ATP in 1x Kinase buffer (50 mM HEPESNaOH, pH 7.5, 150 mM NaCl, 10 mM $MgCl_2$, 1 mM TCEP) on ice for >24 h for maximum autophosphorylation, as confirmed by WB (**Supplementary Fig. 2e,f**). ATP was subsequently removed by gel filtration, and monomeric protein fractions were pooled, snap frozen in liquid $N_2$ and stored at —80 °C. In the case of WT Lck, mass spectrometry analysis revealed 82% phosphorylation for Y394, and 97% phosphorylation for Y505 (**Supplementary Fig. 3**). Notably, the immunoblot analyses have revealed that net phosphate loss of Lck on both regulatory tyrosines can occur at relatively low ATP concentrations (**Supplementary Fig. 2**). Therefore, it is important to incubate Lck with excess concentrations of ATP to achieve maximum and stable level of phosphorylation.

To prephosphorylate CD3ζ for studying the substrate specificity of CD45, $His_{10}$-KKCK-CD3ζ was mixed with $His_{10}$-Lck and ATP in 1x Kinase buffer on ice. Aliquots of reactions were terminated at different time points, and CD3ζ phosphorylation was considered complete when no further changes in electrophoretic mobility were observed. Phosphorylated CD3ζ was then separated with Lck by gel filtration.

### Reconstitution assay of membrane-bound recombinant proteins

Indicated concentrations of $His_{10}$ proteins were premixed and then incubated with DGS-NTA-Ni containing liposomes for 40-60 min to allow for membrane attachment. Following 40 min incubation, $His_{10}$ proteins were undetectable in the supernatant after liposome sedimentation, suggesting complete membrane attachment.

FRET assays were carried out at RT in solid-white 96-well polystyrene plates (Corning) in a total volume of 100 μl per reaction. All protein components (including 0.3 mg/ml BSA in

order to prevent non-specific binding) were mixed, followed by addition of liposomes, and incubated for 40-60 min, during which the SNAP-cell-505 fluorescence was monitored at the minimal intervals (6 s to 30 s, depending on the number of wells monitored) with 504 nm excitation and 540 nm emission. During this period, $His_{10}$ proteins bind to the liposomes and the temperature equilibrates, establishing a stable baseline. ATP was subsequently injected followed by 5 s of automatic shaking of the plate, and the fluorescence was further monitored for at least 1 h. Data were normalized by setting the average fluorescence value of the last 10 data points before ATP addition as 100%, and background fluorescence as 0%.

### Immunoblot analyses of phosphorylation and dephosphorylation

The time course of both phosphorylation (Fig. 2a-c, Fig. 6a,b, Supplementary Fig. 2 and Supplementary Fig. 6) and dephosphorylation (**Fig. 4a)** of Lck was followed by immunoblotting, using mouse mAbs against either pY394 or pY505 of Lck. Autophosphorylation was triggered by 1 mM ATP unless indicated otherwise. For experiments shown in **Fig. 2c**, Lck was reconstituted onto the liposomes at 500 per $\mu m^2$ and autophosphorylation was triggered by indicated concentrations of ATP, terminated after 5 min incubation at RT, and analyzed by WB. The phosphorylation level at 5 min was used as a proxy for the initial rate of autophosphorylation in order to estimate the ATP $K_M$. Experiments shown in **Fig. 4a** were conducted in solution at RT, and dephosphorylation was initiated by adding CD45 (0.1 μM) to a mixture containing equal concentration (0.1 μM) of both prephosphorylated CD3ζ (pCD3ζ) and prephosphorylated Lck (pLck). In all kinetic measurements using immuoblotting, aliquots of reactions were removed and terminated by treating with 1x SDS sample buffer at indicated times, boiled for 5 min, followed by SDS-PAGE and WB using standard protocols. All blots were quantified by ImageJ, if desired.

### Electrophoretic mobility assay for CD3ζ phosphorylation

For experiments shown in **Fig. 3c,d**, DGS-NTA-Ni containing liposomes (1 mM total lipids) were incubated with 20 nM $His_{10}$-Lck plus either 2.54 μM or 7.62 μM $His_{10}$-CD3ζ for 1 h at RT, to achieve the following protein densities: ~58 $\mu m^{-2}$ for $His_{10}$-Lck; ~7,300 or ~22,000 $\mu m^{-2}$ for $His_{10}$-CD3ζ. After the addition of 1 mM ATP, the reaction was terminated at indicated time points and subjected to SDS-PAGE, followed by Coomassie staining.

### Rapamycin-induced protein clustering on membranes

For rapamycin induced CD3ζ-Lck coclustering as shown in **Fig. 7a,b** the two proteins were fused with repeats of FKBP and FRB, respectively, designated as $(FKBP)_6$-CD3ζ and $(FRB)_4$-Lck. These fusion proteins were purified with an N-terminal $His_{10}$-tag and co-attached onto liposomes with CD45. Rapamycin was added 5 min prior to the addition of ATP to induce CD3ζ-Lck coclustering. To measure phase diagrams, the density of $(FRB)_4$-Lck and CD45 was varied, at a fixed density (400 $\mu m^{-2}$) of $(FKBP)_6$-CD3ζ, similar as in **Fig. 5b**. To achieve rapamycin-induced clustering of CD3ζ alone as shown in **Fig. 7c**, 160 $\mu m^{-2}$ $(FKBP)_6$-CD3ζ and 240 $\mu m^{-2}$ $(FRB)_4$-CD3ζ was co-attached to liposomes with various densities of Lck and CD45 (as described in **Fig. 5b**), followed by sequential addition of rapamycin and ATP. The phase diagram data were measured at 1 h after ATP addition. A 2:3 molar ratio of $(FKBP)_6$-CD3ζ and $(FRB)_4$-CD3ζ was used to ensure equal moles of

FKBP and FRB. Final rapamycin concentration was approximately 3-fold of the bulk FKBP concentration. We noted that the efficiency for rapamycin induced clustering exhibits a bell-shaped dependence to rapamycin concentration (E. Hui and R.D. Vale, unpublished observation).

### Liquid chromatography (LC) mass spectrometry

Protein samples were acetone precipitated, followed by reconstitution in freshly prepared 8M urea, 0.2% protease max (Promega), pH 8.0. To mitigate the instability of the phosphate group, as suggested by **Supplementary Fig. 2e,f**, samples were not reduced or alkylated. The urea concentration was diluted to less than 1 M by the addition of 50 mM ammonium bicarbonate, followed by the addition of trypsin at a 1:25 ratio, and allowed to digest for 30 min at 50 °C. A portion of the digest was removed and the reaction was quenched by the addition of 10% formic acid water to a pH < 3. The samples were cleaned using C18 microspin columns (NEST group) and peptides were eluted in 60% acetonitrile, 39.9% water and 0.1% formic acid. The samples were dried in a speed vac briefly, and reconstituted in LC mobile phase A.

The LC was a Proxeon (Thermo) Easy nanoLC II, run at 0.3 μl per min where the column was a self-packed C18 3-μm matrix packed to 15 cm length where the ID was 100 μm. The mass spectrometer was an LTQ Orbitrap Velos in which data was acquired in a data dependent fashion, with the top 12 most intense multiply charged precursor ions selected for fragmentation in the linear ion trap. Data was searched against a custom database containing the sequence of human Lck. Data analysis and extraction, including MS/MS TIC and peptide intensities, were performed using Scaffold (Proteome Software v. 4.05).

### Cell culture and Lck inhibitor treatment

Jurkat T-cell line was kindly provided by Art Weiss (UCSF). Cells were grown in RPMI-1640 (Sigma-Aldrich) supplemented with 5% FBS (Life Technologies), 2 mM L-glutamine, 100 U/ml penicillin and 100 μg/ml Streptomycin and maintained at 37°C with 5% $CO_2$. At $3 \times 10^5$ cells/ml density, Jurkat cells were treated with 100 nM cell-permeable Lck specific inhibitor (4-Amino-5-(4-phenoxyphenyl)-7H-pyrrolo[3,2-d]pyrimidin-7-yl-cyclopentane, Sigma-Aldrich) at 37°C for 0.5 h. $6 \times 10^5$ cells were then harvested by centrifugation at 600 × g for 3 min, and resuspended in 60 ×l lysis buffer (50 mM HEPES-NaOH, pH 7.5, 150 mM NaCl, 0.5% sodium deoxycholate, 1% NP-40, 0.2% SDS, 1 mM $Na_3VO_4$, 10 mM NaF, 1 mM PMSF, 1x complete protease inhibitor (Roche)). After 15 min incubation on ice, cell lysates were centrifuged at 16,000 × g for 10 min, supernatant were removed and mixed with SDS sample buffer, boiled for 5 min, and subjected to SDS-PAGE and WB.

### Protein density calculation

To calculate the surface density of proteins in cells, we assume T cells adopt a spherical shape with 7 μm diameter and all proteins are present on the plasma membranes with a roughness factor of 1.8[62]. Hence 10,000 molecules per cells correspond to ~36 per $\mu m^2$ surface density. The expression levels for Lck, CD45 and TCR have been previously determined and often reported as number of molecules per cell. The number of Lck varies

from 40,000 to 120,000 in T cells[63]. CD45 expression levels vary from 100,000 to 500,000 molecules per cell; TCR level was measured to be 30,000 to 100,000 molecules per cell[64,65]. Based on these previous measurements and the assumptions above, we estimated that the physiological densities for the relevant proteins as follows: CD45 (361-1805 $\mu m^{-2}$), Lck (144-433 $\mu m^{-2}$) and TCR (108-361 $\mu m^{-2}$). T cell normally expresses ~50,000 ZAP70 based on quantitative immunofluorescence measurement (A. Weiss (University of California), personal communication). To mimic physiological conditions, we maintained a 1:1 $SNAP_{505}$-tSH2 to CD3ζ molar ratio in our phase diagram measurements as shown in **Fig. 5-7** and **Supplementary Fig. 5**.

In our reconstitution system, the surface density of a given protein was calculated by dividing the number of protein molecules by the total area of the exposed membranes (outer leaflet) of liposomes. Assuming a 5-nm thickness of the phospholipid bilayer[66], the inner diameter of a 200-nm liposome is 190 nm, therefore ~52.6% of total lipids are present in the outer membranes of liposomes, i.e., for each μmol lipids, ~0.526 μmol are exposed to proteins. Assuming that each phospholipid occupies 0.65 $nm^2$ area[67], the exposed membrane area should be ~$2.06 \times 10^{11}$ $\mu m^2$ per μmol total lipids. Based on the area of occupancy for each phospholipid molecule (0.65 $nm^2$), we can also calculate the total number of lipids per 200-nm liposome (367,000), thereby allowing the calculation of liposome concentration from total lipid concentration in **Supplementary Fig. 1b**.

### Data analyses

The heat maps in **Fig. 5-7** were created in MATLAB 2012b. The % of fluorescence quenching at 1 h after ATP (see **Fig. 5b**) were used to create a 3D-scatter plot with CD45 and Lck densities as *X* and *Y* axis, respectively. The scatter plot was then subjected to delaunay triangulation (*tri = delaunay (X,Y)*), after which a 3D surface plot was generated using the built-in function "*trisurf*". Finally, the 3D surface plot was subjected to rotation to generate the heat map. All dose response data were analyzed with Graphpad Prism 5.0.

### Original images of immunoblots

Original images of immunoblots used in this study can be found in **Supplementary Fig. 9**.

## Supplementary Material

Refer to Web version on PubMed Central for supplementary material.

## ACKNOWLEDGMENTS

We thank A. Weiss (University of California), J. Kuriyan (University of California), Y. Kaizuka (National Institute for Materials Science, Japan), I.A. Yudushkin (University of Vienna, Austria), J.R. James (University of Cambridge, UK), and members of the Vale laboratory for comments and discussions. We acknowledge A. Chien and C. Adams of the Vincent Coates Foundation Mass Spectrometry Laboratory (Stanford University) for LC-MS analyses. R.D.V. is supported as an investigator of the Howard Hughes Medical Institute. E.H. is supported as a fellow of Leukemia & Lymphoma Society.

## REFERENCES


1. Roskoski R Jr. Src kinase regulation by phosphorylation and dephosphorylation. Biochem Biophys Res Commun. 2005; 331:1–14. [PubMed: 15845350]
2. Nada S, Okada M, MacAuley A, Cooper JA, Nakagawa H. Cloning of a complementary DNA for a protein-tyrosine kinase that specifically phosphorylates a negative regulatory site of p60c-src. Nature. 1991; 351:69–72. [PubMed: 1709258]
3. Imamoto A, Soriano P. Disruption of the csk gene, encoding a negative regulator of Src family tyrosine kinases, leads to neural tube defects and embryonic lethality in mice. Cell. 1993; 73:1117–24. [PubMed: 7685657]
4. Sicheri F, Moarefi I, Kuriyan J. Crystal structure of the Src family tyrosine kinase Hck. Nature. 1997; 385:602–9. [PubMed: 9024658]
5. Xu W, Doshi A, Lei M, Eck MJ, Harrison SC. Crystal structures of c-Src reveal features of its autoinhibitory mechanism. Mol Cell. 1999; 3:629–38. [PubMed: 10360179]
6. Hermiston ML, Xu Z, Weiss A. CD45: a critical regulator of signaling thresholds in immune cells. Annu Rev Immunol. 2003; 21:107–37. [PubMed: 12414720]
7. Ostergaard HL, et al. Expression of CD45 alters phosphorylation of the lck-encoded tyrosine protein kinase in murine lymphoma T-cell lines. Proc Natl Acad Sci U S A. 1989; 86:8959–63. [PubMed: 2530588]
8. D'Oro U, Sakaguchi K, Appella E, Ashwell JD. Mutational analysis of Lck in CD45-negative T cells: dominant role of tyrosine 394 phosphorylation in kinase activity. Mol Cell Biol. 1996; 16:4996–5003. [PubMed: 8756658]
9. Baker M, et al. Development of T-leukaemias in CD45 tyrosine phosphatase-deficient mutant lck mice. Embo J. 2000; 19:4644–54. [PubMed: 10970857]
10. Furukawa T, Itoh M, Krueger NX, Streuli M, Saito H. Specific interaction of the CD45 protein-tyrosine phosphatase with tyrosine-phosphorylated CD3 zeta chain. Proc Natl Acad Sci U S A. 1994; 91:10928–32. [PubMed: 7526385]
11. Amrein KE, Sefton BM. Mutation of a site of tyrosine phosphorylation in the lymphocyte-specific tyrosine protein kinase, p56lck, reveals its oncogenic potential in fibroblasts. Proc Natl Acad Sci U S A. 1988; 85:4247–51. [PubMed: 3380789]
12. Mukhopadhyay H, Cordoba SP, Maini PK, van der Merwe PA, Dushek O. Systems model of T cell receptor proximal signaling reveals emergent ultrasensitivity. PLoS Comput Biol. 2013; 9:e1003004. [PubMed: 23555234]
13. Chakraborty AK, Das J. Pairing computation with experimentation: a powerful coupling for understanding T cell signalling. Nat Rev Immunol. 2010; 10:59–71. [PubMed: 20029448]
14. Palacios EH, Weiss A. Function of the Src-family kinases, Lck and Fyn, in T-cell development and activation. Oncogene. 2004; 23:7990–8000. [PubMed: 15489916]
15. Nye JA, Groves JT. Kinetic control of histidine-tagged protein surface density on supported lipid bilayers. Langmuir. 2008; 24:4145–9. [PubMed: 18303929]
16. Adam G, Delbrück M. Reduction of dimensionality in biological diffusion processes. 1968:198–215.
17. Wang D, Gou SY, Axelrod D. Reaction rate enhancement by surface diffusion of adsorbates. Biophys Chem. 1992; 43:117–37. [PubMed: 1498248]
18. Gureasko J, et al. Membrane-dependent signal integration by the Ras activator Son of sevenless. Nat Struct Mol Biol. 2008; 15:452–61. [PubMed: 18454158]
19. Xu C, et al. Regulation of T cell receptor activation by dynamic membrane binding of the CD3epsilon cytoplasmic tyrosine-based motif. Cell. 2008; 135:702–13. [PubMed: 19013279]
20. Shi X, et al. Ca2+ regulates T-cell receptor activation by modulating the charge property of lipids. Nature. 2013; 493:111–5. [PubMed: 23201688]
21. Brugger B, et al. The HIV lipidome: a raft with an unusual composition. Proc Natl Acad Sci U S A. 2006; 103:2641–6. [PubMed: 16481622]
22. Yamaguchi H, Hendrickson WA. Structural basis for activation of human lymphocyte kinase Lck upon tyrosine phosphorylation. Nature. 1996; 384:484–9. [PubMed: 8945479]

23. Veillette A, Latour S, Davidson D. Negative regulation of immunoreceptor signaling. Annu Rev Immunol. 2002; 20:669–707. [PubMed: 11861615]
24. Osusky M, Taylor SJ, Shalloway D. Autophosphorylation of purified c-Src at its primary negative regulation site. J Biol Chem. 1995; 270:25729–32. [PubMed: 7592753]
25. Cooper JA, MacAuley A. Potential positive and negative autoregulation of p60c-src by intermolecular autophosphorylation. Proc Natl Acad Sci U S A. 1988; 85:4232–6. [PubMed: 2454466]
26. Ramer SE, Winkler DG, Carrera A, Roberts TM, Walsh CT. Purification and initial characterization of the lymphoid-cell protein-tyrosine kinase p56lck from a baculovirus expression system. Proc Natl Acad Sci U S A. 1991; 88:6254–8. [PubMed: 2068105]
27. Housden HR, et al. Investigation of the kinetics and order of tyrosine phosphorylation in the T-cell receptor zeta chain by the protein tyrosine kinase Lck. Eur J Biochem. 2003; 270:2369–76. [PubMed: 12755691]
28. Nika K, et al. Constitutively active Lck kinase in T cells drives antigen receptor signal transduction. Immunity. 2010; 32:766–77. [PubMed: 20541955]
29. Scott MP, Miller WT. A peptide model system for processive phosphorylation by Src family kinases. Biochemistry. 2000; 39:14531–7. [PubMed: 11087407]
30. Pellicena P, Miller WT. Processive phosphorylation of p130Cas by Src depends on SH3-polyproline interactions. J Biol Chem. 2001; 276:28190–6. [PubMed: 11389136]
31. Weissenhorn W, Eck MJ, Harrison SC, Wiley DC. Phosphorylated T cell receptor zeta-chain and ZAP70 tandem SH2 domains form a 1:3 complex in vitro. Eur J Biochem. 1996; 238:440–5. [PubMed: 8681956]
32. Patwardhan P, Shen Y, Goldberg GS, Miller WT. Individual Cas phosphorylation sites are dispensable for processive phosphorylation by Src and anchorage-independent cell growth. J Biol Chem. 2006; 281:20689–97. [PubMed: 16707485]
33. Takahashi M, Shibata T, Yanagida T, Sako Y. A protein switch with tunable steepness reconstructed in Escherichia coli cells with eukaryotic signaling proteins. Biochem Biophys Res Commun. 2012; 421:731–5. [PubMed: 22542625]
34. Brdicka T, et al. Phosphoprotein associated with glycosphingolipid-enriched microdomains (PAG), a novel ubiquitously expressed transmembrane adaptor protein, binds the protein tyrosine kinase csk and is involved in regulation of T cell activation. J Exp Med. 2000; 191:1591–604. [PubMed: 10790433]
35. Kawabuchi M, et al. Transmembrane phosphoprotein Cbp regulates the activities of Src-family tyrosine kinases. Nature. 2000; 404:999–1003. [PubMed: 10801129]
36. Schoenborn JR, Tan YX, Zhang C, Shokat KM, Weiss A. Feedback circuits monitor and adjust basal Lck-dependent events in T cell receptor signaling. Sci Signal. 2011; 4:ra59. [PubMed: 21917715]
37. Bunnell SC, et al. T cell receptor ligation induces the formation of dynamically regulated signaling assemblies. J Cell Biol. 2002; 158:1263–75. [PubMed: 12356870]
38. Douglass AD, Vale RD. Single-molecule microscopy reveals plasma membrane microdomains created by protein-protein networks that exclude or trap signaling molecules in T cells. Cell. 2005; 121:937–50. [PubMed: 15960980]
39. Varma R, Campi G, Yokosuka T, Saito T, Dustin ML. T cell receptor-proximal signals are sustained in peripheral microclusters and terminated in the central supramolecular activation cluster. Immunity. 2006; 25:117–27. [PubMed: 16860761]
40. Banaszynski LA, Liu CW, Wandless TJ. Characterization of the FKBP.rapamycin.FRB ternary complex. J Am Chem Soc. 2005; 127:4715–21. [PubMed: 15796538]
41. Li P, et al. Phase transitions in the assembly of multivalent signalling proteins. Nature. 2012; 483:336–40. [PubMed: 22398450]
42. Schamel WW, et al. Coexistence of multivalent and monovalent TCRs explains high sensitivity and wide range of response. J Exp Med. 2005; 202:493–503. [PubMed: 16087711]
43. Lillemeier BF, et al. TCR and Lat are expressed on separate protein islands on T cell membranes and concatenate during activation. Nat Immunol. 2010; 11:90–6. [PubMed: 20010844]

44. Haynes NM, et al. Redirecting mouse CTL against colon carcinoma: superior signaling efficacy of single-chain variable domain chimeras containing TCR-zeta vs Fc epsilon RI-gamma. J Immunol. 2001; 166:182–7. [PubMed: 11123291]
45. Courtneidge SA. Activation of the pp60c-src kinase by middle T antigen binding or by dephosphorylation. Embo J. 1985; 4:1471–7. [PubMed: 2411538]
46. Cooper JA, King CS. Dephosphorylation or antibody binding to the carboxy terminus stimulates pp60c-src. Mol Cell Biol. 1986; 6:4467–77. [PubMed: 2432403]
47. Piwnica-Worms H, Saunders KB, Roberts TM, Smith AE, Cheng SH. Tyrosine phosphorylation regulates the biochemical and biological properties of pp60c-src. Cell. 1987; 49:75–82. [PubMed: 3103926]
48. Kmiecik TE, Shalloway D. Activation and suppression of pp60c-src transforming ability by mutation of its primary sites of tyrosine phosphorylation. Cell. 1987; 49:65–73. [PubMed: 3103925]
49. Cartwright CA, Eckhart W, Simon S, Kaplan PL. Cell transformation by pp60c-src mutated in the carboxy-terminal regulatory domain. Cell. 1987; 49:83–91. [PubMed: 3103927]
50. Kmiecik TE, Johnson PJ, Shalloway D. Regulation by the autophosphorylation site in overexpressed pp60c-src. Mol Cell Biol. 1988; 8:4541–6. [PubMed: 2460746]
51. Sun G, Sharma AK, Budde RJ. Autophosphorylation of Src and Yes blocks their inactivation by Csk phosphorylation. Oncogene. 1998; 17:1587–95. [PubMed: 9794236]
52. Alonso A, et al. Lck dephosphorylation at Tyr-394 and inhibition of T cell antigen receptor signaling by Yersinia phosphatase YopH. J Biol Chem. 2004; 279:4922–8. [PubMed: 14623872]
53. Burchat AF, et al. Pyrrolo[2,3-d]pyrimidines containing an extended 5-substituent as potent and selective inhibitors of lck II. Bioorganic & Medicinal Chemistry Letters. 2000; 10:2171–2174. [PubMed: 11012022]
54. Tan YX, Zikherman J, Weiss A. Novel Tools to Dissect the Dynamic Regulation of TCR Signaling by the Kinase Csk and the Phosphatase CD45. Cold Spring Harb Symp Quant Biol. 2013
55. McNeill L, et al. CD45 isoforms in T cell signalling and development. Immunol Lett. 2004; 92:125–34. [PubMed: 15081536]
56. Ferrell JE Jr. Machleder EM. The biochemical basis of an all-or-none cell fate switch in Xenopus oocytes. Science. 1998; 280:895–8. [PubMed: 9572732]
57. Dushek O, van der Merwe PA, Shahrezaei V. Ultrasensitivity in multisite phosphorylation of membrane-anchored proteins. Biophys J. 100:1189–97. [PubMed: 21354391]
58. Davis SJ, van der Merwe PA. The kinetic-segregation model: TCR triggering and beyond. Nat Immunol. 2006; 7:803–9. [PubMed: 16855606]
59. James JR, Vale RD. Biophysical mechanism of T-cell receptor triggering in a reconstituted system. Nature. 2012; 487:64–9. [PubMed: 22763440]
60. Li H, Korennykh AV, Behrman SL, Walter P. Mammalian endoplasmic reticulum stress sensor IRE1 signals by dynamic clustering. Proc Natl Acad Sci U S A. 2010; 107:16113–8. [PubMed: 20798350]
61. Gaffaney JD, Dunning FM, Wang Z, Hui E, Chapman ER. Synaptotagmin C2B domain regulates Ca2+-triggered fusion in vitro: critical residues revealed by scanning alanine mutagenesis. J Biol Chem. 2008; 283:31763–75. [PubMed: 18784080]
62. Mege JL, et al. Quantification of cell surface roughness; a method for studying cell mechanical and adhesive properties. J Theor Biol. 1986; 119:147–60. [PubMed: 3488469]
63. Olszowy MW, Leuchtmann PL, Veillette A, Shaw AS. Comparison of p56lck and p59fyn protein expression in thymocyte subsets, peripheral T cells, NK cells, and lymphoid cell lines. J Immunol. 1995; 155:4236–40. [PubMed: 7594580]
64. Meuer SC, et al. Evidence for the T3-associated 90K heterodimer as the T-cell antigen receptor. Nature. 1983; 303:808–10. [PubMed: 6191218]
65. Schodin BA, Tsomides TJ, Kranz DM. Correlation between the number of T cell receptors required for T cell activation and TCR-ligand affinity. Immunity. 1996; 5:137–46. [PubMed: 8769477]

66. Wiener MC, White SH. Structure of a fluid dioleoylphosphatidylcholine bilayer determined by joint refinement of x-ray and neutron diffraction data. III. Complete structure. Biophys J. 1992; 61:434–47. [PubMed: 1547331]

67. Cullis, PR.; Fenske, DB.; Hope, MJ. Elsevier; 1996. Biochemistry of Lipids, Lipoproteins and Membranes; p. 1-33.

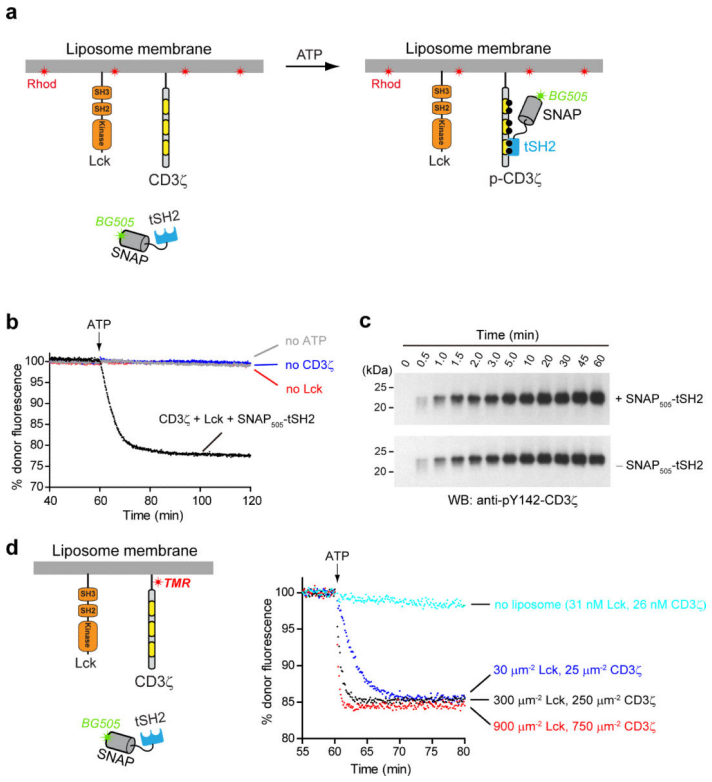


**Figure 1. Lck catalyzed phosphorylation of CD3ζ on liposomes**

**(a)** A cartoon depicting the kinetic, FRET-based assay for monitoring the phosphorylation of CD3ζ on liposomes. The energy donor, SNAP-cell-505, is labeled to SNAP-tag fusion tandem SH2 domain of ZAP70 ($SNAP_{505}$-tSH2). Liposomes harbor polyhistidine chelating lipid DGS-NTA-Ni, and fluorescently labeled lipid Rhod-PE, which serves as the energy acceptor. Phosphorylation of ITAMs recruits $SNAP_{505}$-tSH2 to the membrane, leading to FRET. **(b)** Time course of the fluorescence intensity of $SNAP_{505}$-tSH2 (0.34 μM, 2-fold of CD3ζ bulk concentration) upon incubation with liposome-bound $His_{10}$-Lck (~12 $\mu m^{-2}$) and $His_{10}$-CD3ζ (~500 $\mu m^{-2}$) and addition of 1 mM ATP. **(c)** Western-blot (WB) showing the time course of Lck-catalyzed CD3ζ phosphorylation, in the presence or absence of $SNAP_{505}$-tSH2. Experiment condition was identical to **b** except using immunoblotting rather than fluorescence to follow CD3ζ phosphorylation. Samples were derived from the same experiment and the blots were processed in parallel. Original images of blots are shown in **Supplementary Fig. 9**. **(d)** Comparison of the phosphorylation kinetics in solution ("—liposomes", cyan trace) *versus* on liposomes with three indicated surface densities for Lck and CD3ζ. CD3ζ was labeled with tetramethylrhodamine (FRET donor) via an engineered cysteine (**Online Methods**), and Rhod-PE was omitted from the liposomes. Data shown were successfully repeated in another independent experiment.

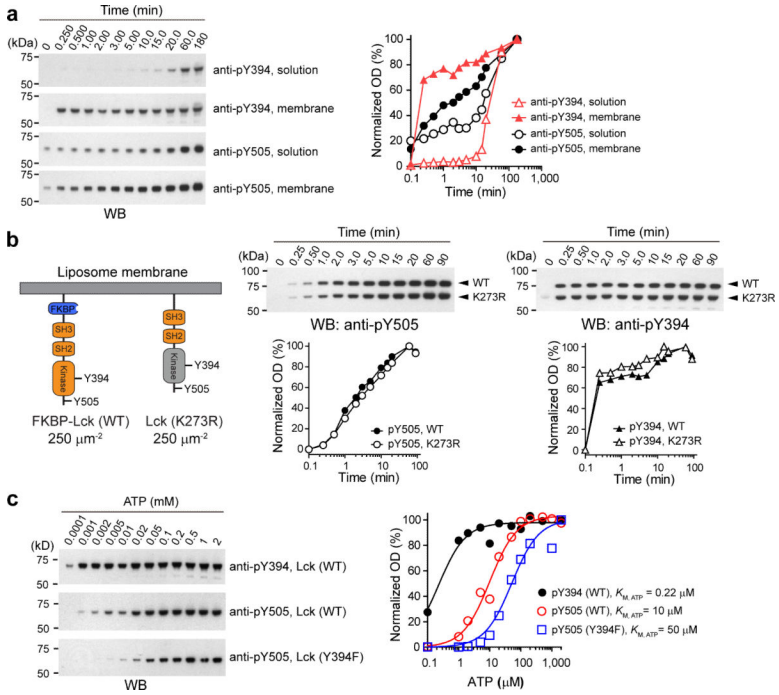


**Figure 2. Lck undergoes autophosphorylation on both Y394 and Y505**

**(a)** Immunoblot analysis of Lck autophosphorylation on membranes *versus* in solution using WB. Left, kinetics of Lck phosphorylation at Y394 and Y505 upon ATP addition, with Lck either in solution (86 nM) or attached on liposomes (~500 Lck per $\mu m^2$, see **Online Methods**). Right, quantification of the immunoblots. Optical density (OD) for each band quantified, normalized to the last time point (180 min) under each condition, and plotted against time. **(b)** Time course of ATP-triggered phosphorylation of WT and kinase-dead Lck (K273R), when both proteins were attached to the same membrane. Left, cartoon showing the two proteins of interested reconstituted at the same density. The 13-kDa FKBP (inserted between $His_{10}$ and Lck) was introduced for electrophoretic separation of WT from kinase-dead Lck. Middle, immunoblots showing the kinetics of Y505 phosphorylation upon ATP addition and the quantification plot. Right, immunoblots showing the kinetics of Y394 phospohorylation upon ATP addition and the quantification plot. **(c)** Immunoblots for measuring the ATP $K_M$ of Lck autophosphorylation at Y394 and Y505 (Lck density: 500 $\mu m^{-2}$). The normalized WB signals at 5 min after ATP addition was plotted against ATP concentration, and fit using Michaelis-Menten model, yielding $K_M$ values. For immunoblots shown in each panel, samples were derived from the same experiment and the blots were processed in parallel. Original images of blots are shown in **Supplementary Fig. 9**.

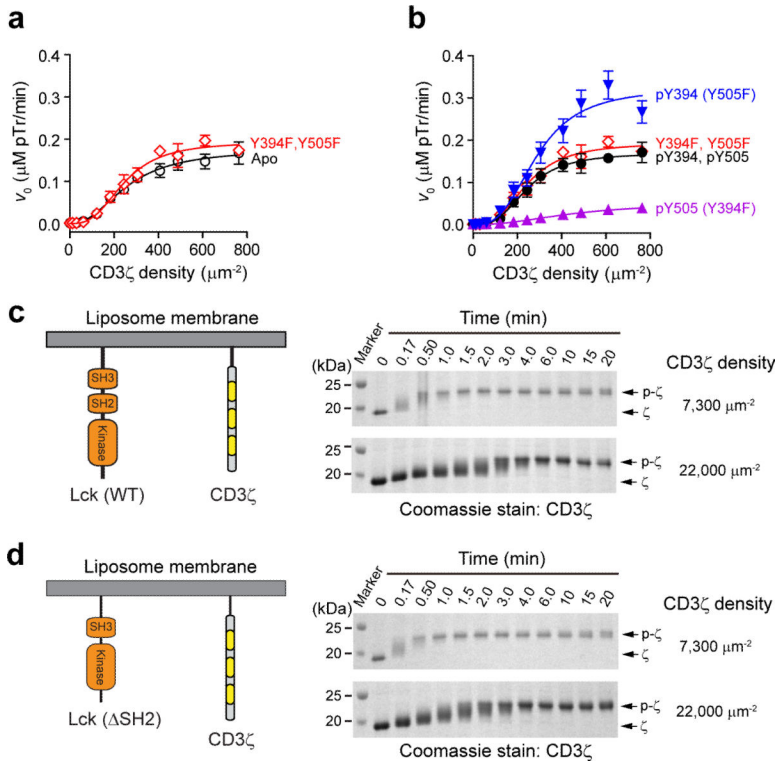


**Figure 3. Enzyme kinetics analyses of Lck catalyzed phosphorylation of CD3ζ**

**(a)** Initial rates ($v_0$) of CD3ζ phosphorylation (determined as shown in **Supplementary Fig. 4**) plotted against CD3ζ surface density for both unphosphorylated Lck (Apo) and the double tyrosine mutant (Y394F, Y505F) of Lck. (**b**) $v_0$-density plots for monophosphorylated Lck-pY394 (Y505F), Lck-pY505 (Y394F), and doubly phosphorylated Lck-pY394-pY505. Data in **a** and **b** were fit by the "allosteric sigmoidal enzyme kinetics" equation using Graphpad Prism 5.0; kinetic parameters were summarized in **Table 1**, error bars: s.e.m., n = 4. **(c,d)** An electrophoretic mobility assay for studying the kinetic mechanism of Lck-catalyzed multisite phosphorylation on CD3ζ, as described in **Online Methods**. Shown are Coomassie-stained SDS-PAGE gels for the time-dependent mobility decrease of CD3ζ, upon addition of 1 mM ATP, indicative of ITAM phosphorylation by Lck. Panel **c** and **d** correspond to two parallel experiments in which WT Lck and Lck (ΔSH2) were used, respectively. All samples were derived from the same experiment and the gels were processed in parallel.

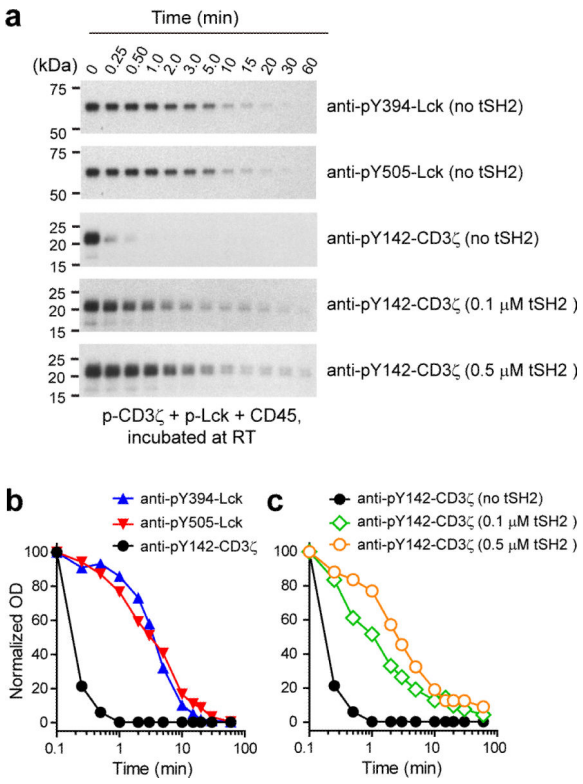


**Figure 4. CD45 substrate specificity in the presence or absence of tSH2 of ZAP70**

**(a)** Immunoblots showing the time course of CD45 catalyzed dephosphorylation of prephosphorylated Lck (pLck) and prephosphorylated CD3ζ (pCD3ζ), in the presence of indicated concentrations of tSH2 of ZAP70, at RT (**Online Methods**) All samples were obtained from the same experiment and the blots were processed in parallel. Original images of blots can be found in **Supplementary Fig. 9**. **(b, c)** Quantification of the immunoblots shown in **a**. The OD of each band normalized to time zero of each condition, and plotted as a function of time. Shown in **b** is a plot comparing the dephosphorylation kinetics of three potential substrates of CD45, in the absence of tSH2. Shown in **c** is a plot comparing the dephosphorylation kinetics of pY-142 of CD3ζ, in the presence of different tSH2 concentrations.

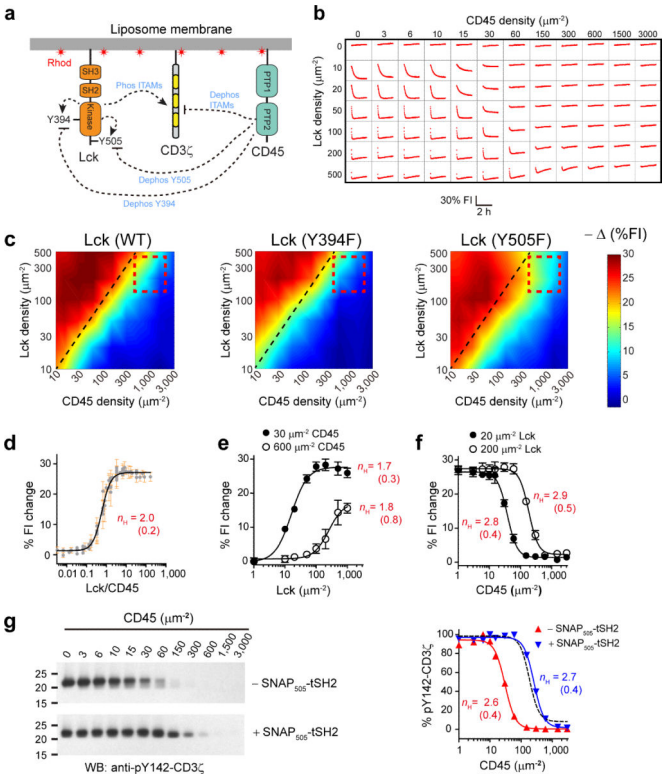


**Figure 5. Phase behavior of the membrane reconstituted Lck-CD45-CD3ζ network**

**(a)** Cartoon depicting the liposome-reconstituted Lck-CD45-CD3ζ network. The dashed arrows indicate potential phosphorylation ("→") and dephosphorylation ("—|") reactions. **(b)** A representative set of time-dependent $SNAP_{505}$-tSH2 fluorescence changes at 84 combinations of Lck and CD45 densities, after ATP addition. **(c)** Heat maps of the Lck-CD45-CD3ζ network with the indicated form of Lck used. % fluorescence quenching (–Δ(%FI)) at 1 h after ATP addition plotted against both Lck and CD45 densities in MATLAB R2012b (**Online Methods**). Black dashed lines: equal Lck and CD45 densities. Red dashed boxes: physiological Lck and CD45 densities. **(d)** % fluorescence quenching for each well pooled, and plotted against the molar ratio of WT Lck over CD45. **(e)** % donor quenching plotted against WT Lck densities for two fixed CD45 densities. **(f)** % donor quenching plotted against CD45 density for two WT Lck densities. (**g**) Reactions as shown in **b** were performed with or without $SNAP_{505}$-tSH2 with 200 $\mu m^{-2}$ Lck and varying CD45. Phosphorylation of Y142-CD3ζ was measured by WB at 1 h, quantified, normalized and plotted against CD45 density. Black dashed line: best-fit of the FRET data in panel **f** (open circles). All data were normalized and fit with sigmoidal dose response curves (variable slopes) with the $n_H$ values indicated (s.e.m. in brackets). Error bars in **d-f**: s.e.m, n = 3. All samples in **g** were derived from the same experiments. Original blots are shown in **Supplementary Fig. 9**.

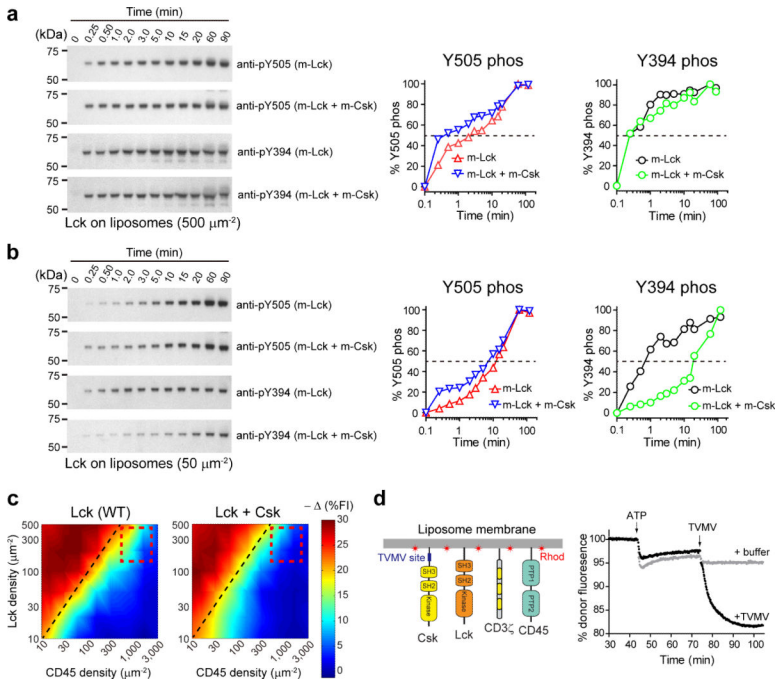


**Figure 6. Csk modulates the phosphorylation of Lck regulatory tyrosines and decreases CD3ζ phosphorylation**

**(a)** Left, immunoblots showing the time course of ATP-triggered phosphorylation of Y394 and Y505 of liposome-bound Lck (~500 $\mu m^{-2}$), with or without liposome-bound Csk (~500 $\mu m^{-2}$). For experiment details, see **Online Methods**. Right, immunoblots quantified, normalized to the last data points (90 min) and plotted against time in a logarithmic scale. The starting signal (time zero) was arbitrary plotted as a data point at 0.1 min. **(b)** Left, immunoblots showing the time course of ATP-triggered phosphorylation of liposome-bound Lck (~50 $\mu m^{-2}$), with or without liposome-bound Csk (~500 $\mu m^{-2}$). Right, quantification plots of immunoblots shown on the left, as described in **a**. All samples in **a,b** were derived from the same experiments. Original images of blots are shown in **Supplementary Fig. 9**. (**c**) Left, a phase diagram for membrane-reconstituted Lck-CD45-CD3ζ network determined as described in **Fig. 4b**, except in the presence of Csk (~150 $\mu m^{-2}$). Right, phase diagram in the absence of Csk (identical to **Fig. 4c**). Black dashed lines: equal levels of Lck and CD45; red dashed boxes: physiological densities of Lck and CD45. **(d)** The time course of $SNAP_{505}$-tSH2 (omitted in the cartoon) fluorescence changes upon sequential addition of ATP (1 mM) and $His_{10}$-TVMV (1 μM). Protein densities on membranes: ~1490 $\mu m^{-2}$ for CD3ζ, ~290 $\mu m^{-2}$ each for Lck, CD45 and Csk.

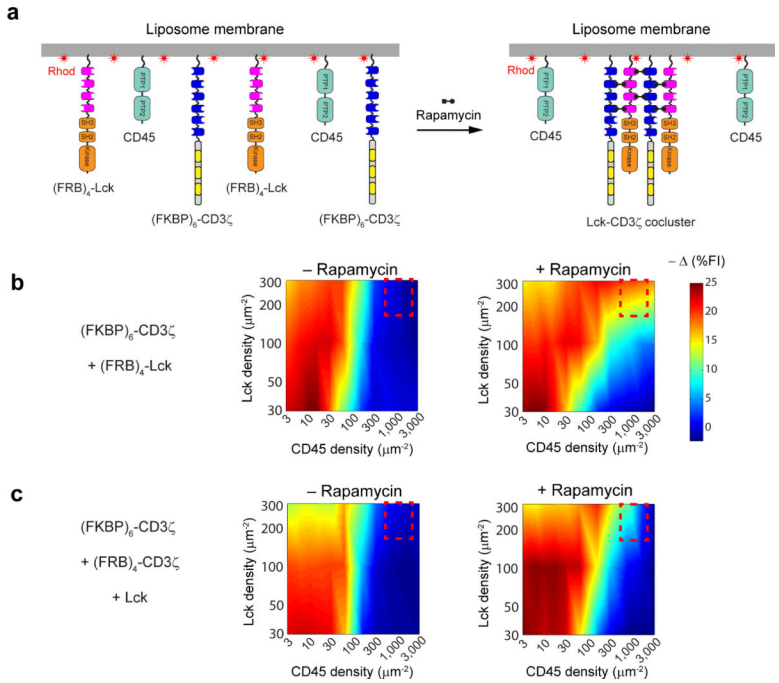


**Figure 7. Protein clustering influences the phase behavior of the TCR proximal signaling network**

**(a)** A cartoon depicting the experimental system for inducing co-clustering of Lck and CD3ζ on liposome membranes. **(b)** Phase diagrams of the membrane-reconstituted kinasephosphatase-CD3ζ network measured under either unclustered (– rapamycin) or Lck-CD3ζ co-clustered (+ rapamycin) conditions. For experiment details, see **Online Methods.** **(c)** Phase diagrams of the membrane-reconstituted kinase-phosphatase-CD3ζ network measured under either unclustered (– rapamycin) or CD3ζ clustered conditions (+ rapamycin). Red dashed boxes denote physiological densities of Lck and CD45.

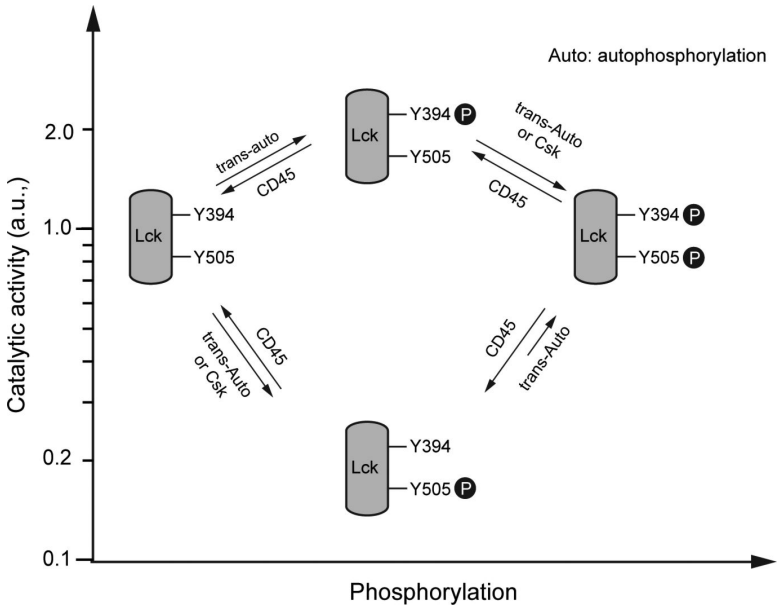


**Figur 8. Model for Lck regulation via tyrosine phosphorylations**

A summary of the relative catalytic activity (logarithmic scale) of Lck for different tyrosine phosphorylation states (the activity of Apo, unphosphorylated Lck was set at “1”). The kinases and phosphatase that promote the reactions are shown. See the Discussion section for details of Lck regulation by phosphorylation.

**Table 1**

2D enzyme-kinetic parameters of Lck at distinct phosphorylation states

| **Proteins** | $K_{M,\,app}$ **(μm$^{-2}$)** | $k_{cat}$ **(s$^{-1}$)** | $k_{cat}/K_{M,app}$ **(×10$^{-2}$ μm$^{-2}$ s$^{-1}$)** | $n_H$ |
|---|---|---|---|---|
| Lck (Apo) | 245 ± 32 | 3.41 ± 0.35 | 1.39 | 2.3 ± 0.5 |
| Lck (Y394F, Y505F) | 234 ± 19 | 3.76 ± 0.27 | 1.61 | 2.9 ± 0.6 |
| Lck-**pY505** (Y394F) | 428 ± 69 | 1.00 ± 0.15 | 0.23 | 2.2 ± 0.4 |
| Lck-**pY394** (Y505F) | 272 ± 65 | 6.26 ± 0.55 | 2.30 | 2.9 ± 0.6 |
| Lck-**pY394-pY505** | 232 ± 19 | 3.29 ± 0.24 | 1.42 | 3.0 ± 0.6 |